

TC-GS: A FASTER GAUSSIAN SPLATTING MODULE UTILIZING TENSOR CORES

Zimu Liao^{1,2} Jifeng Ding^{1,3} Rong Fu^{1,✉} Siwei Cui^{1,4} Ruixuan Gong⁵
 Li Wang⁵ Boni Hu^{1,6} Yi Wang¹ Hengjie Li^{1,7} Xingcheng Zhang¹ Hui Wang¹

¹ Shanghai Artificial Intelligence Laboratory ² Shanghai Jiao Tong University
³ University of Electronic Science and Technology of China ⁴ Fudan University ⁵ Beijing Institute of Technology
⁶ Northwestern Polytechnical University ⁷ Shanghai Innovation Institute



Figure 1: TC-GS: a Tensor Core-based acceleration module for 3D Gaussian Splatting that can be effortlessly applied to existing 3DGS rendering pipelines. Integrated into 3DGS and its variants, it achieves an extra 2x speedup, resulting in an overall 4x acceleration while preserving rendering quality.

ABSTRACT

3D Gaussian Splatting (3DGS) renders pixels by rasterizing Gaussian primitives, where conditional alpha-blending dominates the time cost in the rendering pipeline. This paper proposes TC-GS, an algorithm-independent universal module that expands Tensor Core (TCU) applicability for 3DGS, leading to substantial speedups and seamless integration into existing 3DGS optimization frameworks. The key innovation lies in mapping alpha computation to matrix multiplication, fully utilizing otherwise idle TCUs in existing 3DGS implementations. TC-GS provides plug-and-play acceleration for existing top-tier acceleration algorithms tightly coupled with rendering pipeline designs, like Gaussian compression and redundancy elimination algorithms. Additionally, we introduce a global-to-local coordinate transformation to mitigate rounding errors from quadratic terms of pixel coordinates caused by Tensor Core half-precision computation. Extensive experiments demonstrate that our method maintains rendering quality while providing an additional 2.18x speedup over existing Gaussian acceleration algorithms, thus reaching up to a total 5.6x acceleration. The code are currently available at anonymous <https://github.com/TensorCore3DGS/3DGSTensorCore>.

Keywords Gaussian Splatting · Tensor Cores · Real-Time Rendering

1 Introduction

3D Gaussian Splatting (3DGS) represents a significant advancement in neural rendering, employing Gaussian primitives to achieve NeRF-comparable quality while reducing optimization time to tens of minutes [1, 2]. However, 3DGS rendering speed is heavily constrained by heavy model parameters and inefficient rendering pipelines [3, 4, 5]. Further acceleration remains essential for deployment on resource-constrained devices, real-time large-scale scene rendering systems, and low-latency edge computing scenarios.

Despite numerous efforts to enhance computational efficiency [6, 7, 8, 9], they fail to tap into the most powerful computing units in modern GPUs. Moreover, existing acceleration modules are tightly coupled with core components, preventing modular reuse and cross-method adaptation. This coupling further limits the practical deployment and scalability of 3DGS-based solutions.

Recent research [6, 7, 8, 9] has identified the *conditional alpha-blending* process as the primary pipeline bottleneck, which composites pixel colors with depth-sorted splatted Gaussian primitives. This process comprises three steps: (1) *Alpha computation*: computing the alpha value (opacity) of each splatted Gaussian fragment on the pixel; (2) *Culling*: eliminating fragments with low alpha values; and (3) *Blending*: compositing remaining fragments into final pixel colors. Many approaches [10, 6, 11] employ early culling strategies to reduce the range of splatted Gaussians, thereby minimizing redundant alpha-blending computations. Although eliminating redundant tile computation, they require corresponding pipeline designs to mitigate load imbalance issues introduced by precise intersection [7], or sacrifice certain accuracy [6]. Additionally, we observe that over 80% of Gaussian-pixel pairs requiring culling still remain in the pipeline. Consequently, the first two steps are the dominant part of the alpha-blending process.

Unlike previous efforts to remove redundant computing [6, 7, 8, 9], we focus on utilizing Tensor Core Units (TCUs) for accelerating alpha computation, which remains an unexplored area. In modern GPUs, TCUs are deployed to perform matrix multiply accumulate (MMA), i.e., $D = A \times B + C$ operation within a single clock cycle, achieving high throughput on general matrix multiplication (GEMM) based computations including MLPs, CNNs, and transformers [12]. However, due to their specialized computation pattern, TCUs struggle to be applied to non-GEMM computations, leaving them idle in 3DGS.

To tackle this problem, this paper proposes TC-GS, a hardware-aligned redesign of alpha computation that unlocks Tensor Core acceleration for all 3DGS algorithms. TC-GS formulates a mapping from pixels and Gaussians into two matrices, where their matrix product yields logarithmic alpha values in batches. Implemented as a standalone module, TC-GS not only significantly improves rendering efficiency but also enables seamless integration with existing 3DGS acceleration kernels, further enhancing overall performance.

In summary, the paper proposes the following contributions:

- Our detailed runtime analysis of the rendering pipeline proves that alpha computation in conditional alpha-blending is the performance bottleneck of the 3DGS inference rendering.
- TC-GS is the first to expand Tensor Core applicability for 3DGS, through mapping the alpha computation into matrix multiplication, enabling full utilization of otherwise idle TCUs in existing 3DGS implementations. As an algorithm-independent acceleration module, TC-GS seamlessly integrates into diverse 3DGS acceleration kernels and frameworks to achieve more efficient rendering performance.
- We introduce a global-to-local coordinate transformation (G2L) that reduces the absolute magnitudes of quadratic coordinate terms, which are sensitive to Tensor Core half-precision computation, enabling lossless rendering quality while maintaining full acceleration benefits.

2 Related Works

2.1 Fast 3D Gaussian Splatting

3DGS [13] has emerged as a leading real-time rendering technique with its photo-realistic visual quality, finding a wide range of applications including autonomous driving [14], robotics [15], virtual reality [5]. Current acceleration research explores two primary optimization strategies to enhance 3DGS performance. The first strategy involves modifying the algorithm itself to achieve better efficiency [10, 1, 16]. CompactGS [16] and gsplat [10] introduce more efficient radiance field representations and adaptive resolution primitive pruning algorithms, while Taming-3DGS [1] presents mathematically equivalent but computationally efficient solutions for gradient computation and attribute updates, substantially accelerating training speed. The second category focuses on improving computational efficiency of the original algorithm through intelligent task scheduling and CUDA kernel optimization [7, 8, 6, 10, 17, 2]. Balanced-3DGS [17] optimizes the forward computation of rendering CUDA kernels within warps while minimizing thread idle

Table 1: Tensor Core & CUDA Core Comparision among various GPUs. * stands for using new sparse feature

GPU	Peak FP16	Peak FP16 Tensor Core
H100 (PCIe)	96 TFLOPS	800 TFLOPS 1600 TFLOPS*
A100	78 TFLOPS	312 TFLOPS 624 TFLOPS*
V100	31.4 TFLOPS	125 TFLOPS
RTX 4090	82.6 TFLOPS	330.3 TFLOPS 660.6 TFLOPS*

time and maximizing resource utilization by evenly distributing tasks across compute blocks. Several works, including AdRGaussian [6], FlashGS [7], and SpeedySplat [8], aim to reduce the number of pixels processed per Gaussian by designing more precise Gaussian-tile bounding boxes, with FlashGS [7] and SpeedySplat [8] further computing exact Gaussian-tile intersections. DISTWAR [2] enhances processing efficiency through sophisticated thread management strategies, fully leveraging warp-level reductions in SM sub-cores and intelligently distributing atomic computations between SM and L2 atomic units based on memory access patterns. While these methods significantly accelerate training or rendering speed, strong coupling between algorithmic modules hinders transferability and reusability. Moreover, they fail to leverage modern hardware acceleration features such as Tensor Cores, further limiting the practical deployment and scalability of 3DGS solutions.

2.2 Tensor Cores for Non-GEMM Based Computations

Tensor Cores Units are specialized hardware units developed by NVIDIA to accelerate Deep Learning applications [18]. Each Tensor Core can perform a matrix multiply accumulate operation $D = A \times B + C$ on small matrices within a GPU cycle, where A and B must be in half percision format while the accumulators, C and D, can be either single or half percision. Tensor Core can achieve higher throughput than normal CUDA Cores: for instance on the NVIDIA A100 GPU, CUDA Cores has maximum 78 TFLOPS fp16 performance, whereas Tensor Cores can achieve 312 TFLOPS which is $4\times$ times faster than CUDA Cores.

Despite this theoretical advantage, it is not a trival task to exploit Tensor Cores in arbitrary applications since Tensor Cores only support the matrix–multiply–accumulate (MMA) instruction rather than the full range of CUDA instructions set. This restriction demands that algorithms be reformulated in terms of small matrix operations, but the reward is exceptionally fast execution. Consequently, the strict requirements yet remarkable speed of Tensor Core operations have attracted researchers to explore adapting non-machine learning algorithms to GPU Tensor Cores, leveraging their performance potential. Previous work has efficiently mapped reduction and scan primitives to Tensor Cores[19, 20].Recently ConvStencil[21] has managed to adapt stencil computation to TCU. However, to our best knowledge, no prior work has explored how to exploit Tensor Cores directly within a 3D Gaussian Splatting rendering pipeline.

3 Preliminaries and Observations

3.1 3DGS Rendering Pipeline

A 3DGS model consists of a set of 3D Gaussians primitives $\mathcal{G} = \{G^{(1)}, G^{(2)}, \dots, G^{(P)}\}$. Each Gaussian $G : \mathbb{R}^3 \rightarrow \mathbb{R}$ is parameterized by its mean $\mu \in \mathbb{R}^3$, semi-definite covariance $\Sigma \in \mathbb{R}^{3 \times 3}$, opacity $o \in (0, 1]$, and color $c \in [0, 1]^3$ and maps any 3D position $x \in \mathbb{R}^3$ to its density:

$$G(x) = oe^{-\frac{1}{2}(x-\mu)^T \Sigma^{-1}(x-\mu)}. \quad (1)$$

The inference procedure of 3DGS can be divided into the following 3 stages:

Preprocess The preprocess stage projects 3D Gaussians into 2D planes in parallel according to the viewing transform W of a given camera:

$$\mu' = W\mu \in \mathbb{R}^2, \quad \Sigma' = JW\Sigma W^T J^T \in \mathbb{R}^{2 \times 2}, \quad (2)$$

where $J = \frac{\partial \mu'}{\partial \mu}$ is the Jacobian of projection W . The complexity of the preprocess stage is $\mathcal{E}_p = O(P)$, where P is the number of Gaussians.

Sorting For each projected Gaussian, this stage identifies all the tiles it covers. Then, for each tile $\mathcal{T} \in \mathcal{S}$, the overlapped Gaussians are sorted by depth. A tile \mathcal{T} coupled with a covering Gaussian G' is denoted as a **splat** (\mathcal{T}, G') .

The total number of splats given by

$$N = \sum_{i=1}^P \sum_{\mathcal{T} \in \mathcal{S}} \mathbf{1}(\mathcal{T} \cap G^{(i)} \neq \emptyset) = \sum_{\mathcal{T} \in \mathcal{S}} n(\mathcal{T}), \quad (3)$$

where $\mathbf{1}$ is the indicator function that checks whether the Gaussian covers the tile. The process of determining coverage depends on the specific algorithm used. The complexity of the sorting stage is $\mathcal{E}_s = O(dN)$, where $d = 64$ is the coefficient in radix-sort.

Algorithm 1: Conditional Alpha-blending

Input: Tile \mathcal{T} , Sorted Gaussians $\mathcal{G}'(\mathcal{T}) = (G^{(1)}, \dots, G^{(n(\mathcal{T}))})$

Output: Pixel colors $C_{\mathcal{T}} = (C_1, \dots, C_{|\mathcal{T}|})$

for pixel $p \in \mathcal{T}$ **in parallel** **do**

$T \leftarrow 1$; // Initialize transmissivity
 $C \leftarrow (0, 0, 0)$; // Initialize RGB

foreach Gaussian $G' \in \mathcal{G}'(\mathcal{T})$ **do**

$\alpha \leftarrow o \exp\left(-\frac{1}{2}(\mu' - p)^T \Sigma'^{-1}(\mu' - p)\right)$

if $\alpha < \frac{1}{255}$ **then**

continue; ;

// Cull invisible Gaussians

end

if $T - \alpha T < 0.0001$ **then**

break; ;

// Terminate blending

end

$C \leftarrow C + c\alpha T$;

// Composite colors

$T \leftarrow T - \alpha T$;

// Update transmissivity

end

end

Conditional Alpha-blending This stage renders the final color of each pixel in a tile $\mathcal{T} = (p_1, p_2, \dots, p_{|\mathcal{T}|})$ in parallel as Algorithm 1. Initially, for each projected overlapping Gaussian, the renderer will compute the local opacity $\alpha_i^{(j)}$ at each pixel $p_i = (p_{x_i}, p_{y_i})$:

$$\alpha_i^{(j)} = o^{(j)} \exp\left(-\frac{1}{2}(\mu'^{(j)} - p_i)^T (\Sigma'^{(j)})^{-1}(\mu'^{(j)} - p_i)\right). \quad (4)$$

Next, the renderer performs **culling** of Gaussians at each pixel if the local opacity is below a threshold:

$$\alpha_i^{(j)} < \frac{1}{255}, \quad (5)$$

Otherwise, the surviving Gaussians will contribute the pixel's color:

$$C_i = \sum_{j=1}^{n(\mathcal{T})} c^{(j)} \alpha_i^{(j)} T_i^{(j)}, \quad T_i^{(j)} = \prod_{k=1}^{j-1} (1 - \alpha_i^{(k)}). \quad (6)$$

where $T_i^{(j)}$ denotes the transmissivity and $n(\mathcal{T})$ is the number of splats of the tile \mathcal{T} . If $T_i^{(j)} < 0.0001$, the renderer will **terminate** the blending process for that pixel and output the color. A pixel p rendered by a Gaussian G is referred to as a **fragment**, (p, G) .

Thus, the total complexity of the Gaussian rasterization pipeline can be summarized as $\mathcal{E} = \mathcal{E}_p + \mathcal{E}_s + \mathcal{E}_a$, where $\mathcal{E}_p, \mathcal{E}_s, \mathcal{E}_a$ represent the complexities of preprocess, sorting, and alpha-blending stages, respectively.

3.2 Runtime Analysis

To better understand the bottlenecks in current rendering methods, we conduct a detailed time breakdown analysis of the three stages mentioned above. Specifically, we profile 3DGS, AdR-Gaussian, and Speedy-Splat on an NVIDIA A800 using multiple datasets. While recent methods incorporate early culling strategies with more precise intersection

checks to reduce the number of splats N , thereby decreasing the time spent on sorting and blending, the alpha blending stage still remains the dominant contributor to the overall rendering time, as shown in the bottom-left corner of Figure 3.

Motivated by this observation, we further analyze the core kernel `renderCUDA`, which implements the alpha blending stage, in order to uncover deeper inefficiencies and guide targeted improvements.

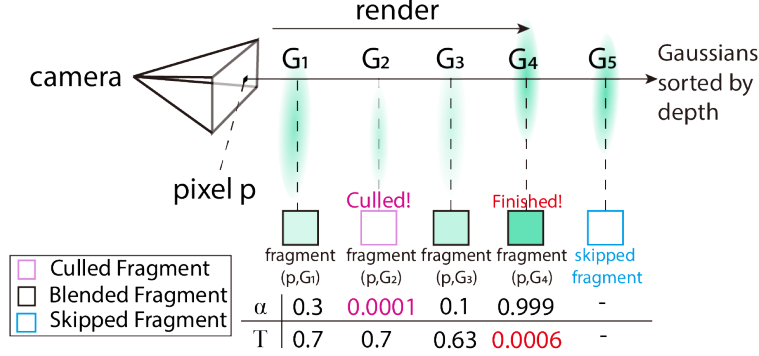


Figure 2: a) Three types of fragments on a pixel. b) If the Gaussian only covers a small portion of tile, a large amount culled fragments are generated.

The alpha-blending stage will blend all fragments into pixel colors. These fragments are categorized into 3 types as Figure 2 shows:

- **Culled fragments:** Fragments that are discarded because $\alpha < \frac{1}{255}$. As shown in Figure 2, the second fragment is culled.
- **Blended fragments:** Fragments that contribute to the final pixel colors. As shown in Figure 2, the first, third, and fourth fragments are blended.
- **Skipped fragments:** Fragments that are ignored when $T < 0.0001$, causing the renderer to terminate the blending process for the corresponding pixel. As shown in Figure 2, the fifth fragment and the ones that follow are skipped. There is no computation on skipped fragments.

Table 2: The alpha computation and culling steps are run on both blended and culled fragments, while the blending step is only performed on blended fragments. There is no computation on skipped fragments.

Fragments	Alpha Computation	Culling	Blending
Blended	✓	✓	✓
Culled	✓	✓	
Skipped			

To model the computation for each type of fragments, we denote $k_\alpha, k_{\text{cull}}, k_{\text{blend}}$ as the average computation cost for alpha computation, culling, and blending. Similarly, let $f_{\text{blend}}, f_{\text{cull}}, f_{\text{skip}}$ represent the number of blended, culled and skipped fragments. According to Table 2, the total computation amount is:

$$\mathcal{C} = k_{\text{blend}}f_{\text{blend}} + (k_{\text{cull}} + k_\alpha)(f_{\text{blend}} + f_{\text{cull}}). \quad (7)$$

To identify the bottleneck within the alpha-blending stage, we collect and categorize the generated fragments on various scenes using 3DGS, AdR-Gaussian and Speedy-Splat. As shown on the right side of Figure 3, culled and skipped fragments account for a large proportion. Since skipped fragments do not incur any computational cost, we can preliminarily conclude that the bottleneck lies in the alpha computation and culling steps.

4 Method

This section introduces how TC-GS utilizes the Tensor Cores to accelerate the alpha-computation and culling process, which are the bottlenecks of rendering. The fundamental components of TC-GS include *frag2Mat* for matrix transformation and *G2L* for coordinate transformation. The detailed design is shown in Figure 4.

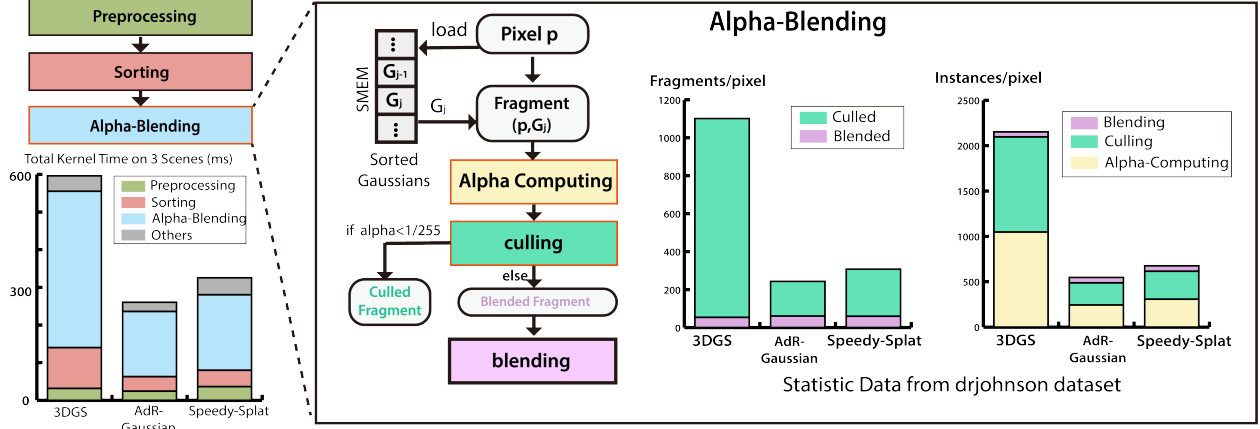


Figure 3: Analysis of 3DGS rendering bottlenecks: The left side shows the time distribution of preprocessing, sorting, and alpha-blending for 3DGS, AdR-Gaussian, and Speedy-Splat, with alpha-blending dominating. The right side details alpha computation, culling, and blending, identifying culled fragments as the primary bottleneck due to redundant alpha computations, while skipped fragments incur no cost.

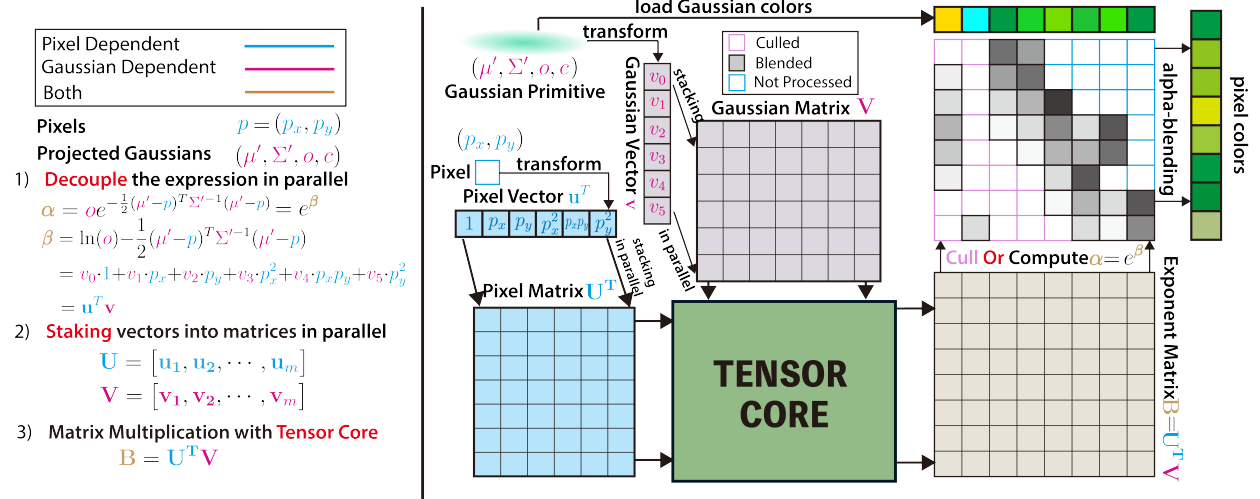


Figure 4: Design of *frag2Mat*: the alpha computation is reformulated as matrix multiplication to fully leverage Tensor Cores for accelerating alpha calculation.

4.1 Batched Exponents Computation with Tensor Cores: Fitting the MMA Operation

While Tensor Cores specialize in matrix multiply-accumulate (MMA) operations, the original alpha-computation involves per-pixel-per-Gaussian evaluations that exhibit non-coalesced memory access patterns and fragmented arithmetic operations – characteristics mismatched with matrix-oriented hardware architectures. To align with Tensor Cores’ computational paradigm and fully exploit their high throughput, we restructure the alpha-computation into batched matrix operations through algebraic reformulation.

We propose *frag2Mat*, a computational restructuring that transforms per-pixel-per-Gaussian exponent calculations into unified matrix operations. By expressing the exponent as a linear combination of pixel coordinates, Gaussian parameters and their quadratic terms, we decouple multivariate dependencies into two independent components: a pixel vector encoding coordinate polynomials for its pixel, and a Gaussian vector composed of parameters from its Gaussian. The final exponent values are batch-calculated through standard matrix multiplication of two matrices formed by stacking pixel vectors and Gaussian vectors respectively.

Firstly, TC-GS converts Equation 4 into $\alpha_i^{(j)} = \exp(\beta_i^{(j)})$, where

$$\beta_i^{(j)} = \ln(o^{(j)}) - \frac{1}{2}(\mu'^{(j)} - p_i)^T (\Sigma'^{(j)})^{-1} (\mu'^{(j)} - p_i). \quad (8)$$

The core idea of TC-GS is decoupling the computation of exponents $\beta_i^{(j)}$ into two separated terms: one that depends only on the pixel index and another that depends only on the Gaussian. Notably, we observe that the exponent can be expressed as a quadratic function of the pixel p . Based on this observation, TC-GS transforms Equation 8 into the following standard form:

$$\beta_i^{(j)} = v_0^{(j)} + v_1^{(j)} p_{x_i} + v_2^{(j)} p_{y_i} + v_3^{(j)} p_{x_i}^2 + v_4^{(j)} p_{x_i} p_{y_i} + v_5^{(j)} p_{y_i}^2, \quad (9)$$

where

$$\begin{aligned} v_0^{(j)} &= \ln(o^{(j)}) - \frac{1}{2}(\mu'^{(j)})^T (\Sigma'^{(j)})^{-1} \mu'^{(j)}, \\ v_1^{(j)} &= a^{(j)} \mu_x^{(j)} + b^{(j)} \mu_y^{(j)}, \quad v_2^{(j)} = b^{(j)} \mu_x^{(j)} + c^{(j)} \mu_y^{(j)}, \\ v_3^{(j)} &= -\frac{1}{2}a^{(j)}, \quad v_4^{(j)} = -b^{(j)}, \quad v_5^{(j)} = -\frac{1}{2}c^{(j)} \end{aligned} \quad (10)$$

with the notation that $\Sigma'^{-1} = \begin{bmatrix} a & b \\ b & c \end{bmatrix}$. The Equation 9 is the expanded dot product of two vectors:

$$\beta_i^{(j)} = \mathbf{u}_i^T \mathbf{v}^{(j)}, \quad (11)$$

where

$$\mathbf{u}_i = [1 \quad p_{x_i} \quad p_{y_i} \quad p_{x_i}^2 \quad p_{x_i} p_{y_i} \quad p_{y_i}^2]^T \quad (12)$$

and

$$\mathbf{v}^{(j)} = [v_0^{(j)} \quad v_1^{(j)} \quad v_2^{(j)} \quad v_3^{(j)} \quad v_4^{(j)} \quad v_5^{(j)}]. \quad (13)$$

Here \mathbf{u}_i , the pixel vector solely dependent on pixel properties, which will be computed only *once* for each pixel. Similarly, each Gaussian vector $\mathbf{v}^{(j)}$ can be only computed once. Therefore, the expression of the exponent is decoupled into the dot product of two individual vectors. To align the computation to the Tensor Cores, TC-GS stacks the vectors into two independent matrices:

$$\mathbf{U} = [\mathbf{u}_1 \quad \mathbf{u}_2 \quad \dots \quad \mathbf{u}_m] \in \mathbb{R}^{6 \times m}, \quad (14)$$

$$\mathbf{V} = [\mathbf{v}^{(1)} \quad \mathbf{v}^{(2)} \quad \dots \quad \mathbf{v}^{(n)}] \in \mathbb{R}^{6 \times n}, \quad (15)$$

where m is the the number of pixels within a tile, and n is the number of Gaussians whose projection is overlapped with the tile. Then TC-GS computes the exponent matrix $\mathbf{B} \in \mathbb{R}^{m \times n}$ as matrix multiplication:

$$\mathbf{B} = \begin{bmatrix} \beta_1^{(1)} & \dots & \beta_1^{(n)} \\ \vdots & \ddots & \vdots \\ \beta_m^{(1)} & \dots & \beta_m^{(n)} \end{bmatrix} = \begin{bmatrix} \mathbf{u}_1^T \mathbf{v}^{(1)} & \dots & \mathbf{u}_1^T \mathbf{v}^{(n)} \\ \vdots & \ddots & \vdots \\ \mathbf{u}_m^T \mathbf{v}^{(1)} & \dots & \mathbf{u}_m^T \mathbf{v}^{(n)} \end{bmatrix} = \mathbf{U}^T \mathbf{V}. \quad (16)$$

Therefore, we can leverage Tensor Cores to compute β for m pixels and n Gaussians simultaneously. As Tensor Cores natively support half-precision matrix operations, additional design is required to ensure numerical stability throughout the alpha computation.

4.2 Transform Global to Local Coordinates: Fitting the Half Precision

Although we adopted Tensor Cores for alpha computation and culling. The challenges remain as Tensor Cores do not support common single-precision floating-point operations. Instead, they only take FP16 or TF32 as the input of the MMA operation, resulting in a higher machine epsilon of $\epsilon_H = 9.77 \times 10^{-4}$ compared to FP32's $\epsilon_F = 1.19 \times 10^{-7}$. The rounding error of a floating number r is $|r| \times \epsilon_H$. Therefore, the error of computation on Tensor Cores is more sensitive at the absolute value of the input data.

We notice that the range of the pixel p is $[0, w] \times [0, h]$, where w, h are the width and height of the screen space, respectively. When loading the pixel vector \mathbf{u} in Equation 12 into Tensor Cores, its absolute values of quadratic terms p_x^2 , $p_x p_y$ and p_y^2 can exceed a million, contributing catastrophic rounding errors to β , whose relative error is more than 35000% at the resolution of 720p as proved on Appendix B.1. Moreover, overflow will occur if the FP16 range $[-6.55 \times 10^5, 6.55 \times 10^5]$ is used.

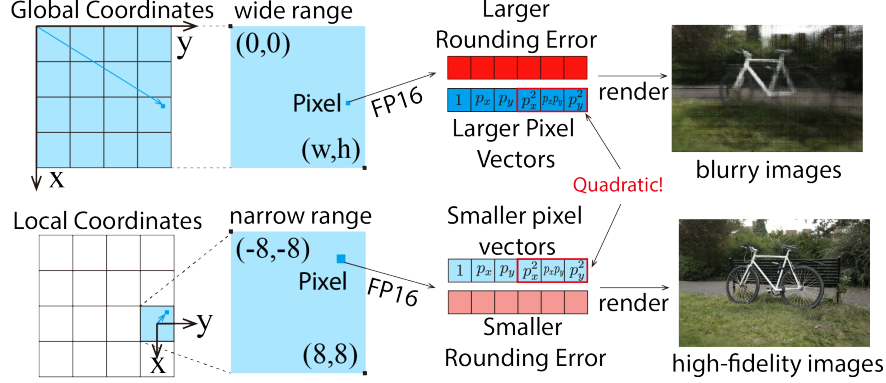


Figure 5: The quadratic term of pixel coordinates significantly contributes the rounding error, resulting in blurry images. Local coordinates constrain the value of Δp into $[-8, 8]^2$, which can reduce the upper bound of the rounding error.

To tackle this problem, TC-GS has designed G2L, a coordinate mapping, which significantly reduces the absolute value of terms in pixel vectors. Since all pixels p within a tile \mathcal{T} will be rendered in parallel, G2L can map the coordinates of pixels into the local coordinate:

$$\Delta p = p - p(\mathcal{T}), \quad (17)$$

Since each tile contains 16×16 pixels, then the range of pixel in LC is $\Delta p \in [-8, 8]^2$, and the maximum element of \mathbf{u}_Δ will not exceed 64. This conversion does not only avoid the overflow in FP16, but also significantly reduces the rounding error.

Respectively, the means of Gaussians in the local coordinate is

$$\Delta \mu' = \mu' - p(\mathcal{T}). \quad (18)$$

Notice that the relative position between μ' and p stays invariant:

$$\Delta \mu' - \Delta p = \mu' - p. \quad (19)$$

Therefore, frag2Mat can be also performed on local coordinates. As the proof in Appendix B goes, G2L reduces the quadratic rounding error $O(h^2 + hw + w^2)$ into linear $O(h + w)$, and achieve better rendering quality in FP16 as Section 5.3 demonstrates.

4.3 Implementation Details

TC-GS also incorporates several common optimization techniques to further enhance overall performance.

First, TC-GS adopts an early-pruning strategy: it identifies invisible Gaussians that can be culled before the alpha-computation stage, greatly reducing the number of exponential (exp) instructions executed and improving throughput.

We begin by expressing the exponentiation in logarithmic form, allowing us to precompute each Gaussian’s opacity during the preprocessing stage. This lets us filter out non-contributing Gaussians in advance, reducing the amount of exp instructions issued by alpha computation. Since prior experiments show that culled fragments account for a large portion of the workload, this approach yields a substantial speed-up for the entire pipeline.

Additionally, TC-GS precisely arranges the shared-memory layout to minimize bank conflicts during warp-level shared-memory reads and writes. This maximizes the operator’s effective bandwidth and fully unleashes Tensor Core performance.

5 Experiment

5.1 Experiment Setup

datasets&metrics To prove that our method is universal and efficient, we conduct experiments on the same datasets as those used in 3DGS[13]. Specifically, the datasets contain all scenes from Mip-NeRF360[22], two outdoor scenes (Truck & Train) from Tanks & Temple[23], two indoor scenes (Drjohnson & playroom) in Deep-Blending[24]. For each scene, CUDA events are inserted at the start and end of the forward rendering procedure to measure FPS values, and the reported results represent the average metrics of the test datasets. All experiments are conducted on an NVIDIA A800 GPU (80GB SXM) equipped with 432 Tensor Cores, achieving a peak 624 TFLOPS FP16 performance.

Table 3: Comparison With/Without TC-GS Module Across Datasets

Method	Tanks & Temple				Deep-Blending				Mip-NeRF360			
	FPS↑	PSNR↑	SSIM↑	LPIPS↓	FPS↑	PSNR↑	SSIM↑	LPIPS↓	FPS↑	PSNR↑	SSIM↑	LPIPS↓
3DGS	161.548	23.687	0.851	0.169	131.373	29.803	0.907	0.238	128.88	26.546	0.785	0.25
3DGS(+TC-GS)	323.423(2.13×)	23.682	0.851	0.169	286.819(2.185×)	29.803	0.906	0.236	258.809(2.01×)	26.544	0.785	0.25
FlashGS	326.835	23.706	0.851	0.169	563.590	29.789	0.907	0.239	399.772	26.551	0.786	0.251
FlashGS(+TC-GS)	539.387(1.65×)	23.684	0.851	0.169	735.777(1.305×)	29.806	0.906	0.236	479.338(1.199×)	26.508	0.785	0.25
Speedy-Splat	268.602	23.687	0.852	0.17	315.822	29.803	0.907	0.238	264.23	26.546	0.785	0.25
Speedy-Splat(+TC-GS)	521.284(1.94×)	23.684	0.852	0.169	579.988(1.84×)	29.802	0.906	0.236	465.308(1.76×)	26.544	0.785	0.25
AdR-Gaussian	278.65	23.635	0.852	0.17	324.18	29.814	0.907	0.238	261.339	26.52	0.785	0.25
AdR-Gaussian(+TC-GS)	545.154(1.955×)	23.632	0.851	0.169	612.063(1.89×)	29.815	0.906	0.236	467.310(1.78×)	26.519	0.785	0.25

Table 4: Comparison of alpha-blending time across methods and datasets.

Method	Scene	with TC-GS time(ms)	original time(ms)
3DGS	drjohnson	1.348(3.49×)	4.705
	train	1.217(3.57×)	4.348
	flowers	0.880(3.68×)	3.236
FlashGS	drjohnson	0.540(2.18×)	1.179
	train	0.609(2.03×)	1.234
	flowers	0.625(2.38×)	1.487
AdR-Gaussian	drjohnson	0.406(4.76×)	1.931
	train	0.518(4.23×)	2.191
	flowers	0.469(4.39×)	2.061
Speedy-Splat	drjohnson	0.510(3.86×)	1.969
	train	0.672(3.46×)	2.326
	flowers	0.592(3.52×)	2.083

5.2 Comparisons

TC-GS demonstrates significant performance improvements in all tested methods while keeping rendering quality. The qualitative and quantitative comparison between four baseline rendering pipelines and their results after integrating the TC-GS module are shown in Table 3.

Rendering speed Across all datasets, incorporating the TC-GS module roughly **doubles** frame throughput except for FlashGS. The state-of-the-art performance is attained by FlashGS integrated with TC-GS, which achieves a **3.3–5.6×** speedup compared to the original 3DGS, while delivering rendering speeds of **479.3–735.8 FPS**.

By comparing the performance of alpha-blending, as shown in Figure 4, the rendering pipeline gains a 2–4× performance improvement. Combined with the previous analysis, this further emphasizes the importance of optimizing the rendering pipeline.

While AdR-Gaussian and Speedy-Splat already employ advanced optimizations to reduce redundant computation, TC-GS further pushed their performance boundaries, delivering significant speedup of **1.87×** and **1.84×** respectively. As for FlashGS, while its existing pipeline rendering optimizations yield a more modest 1.38× average acceleration with TC-GS integration, we emphasize that the pipeline optimizations and TC-GS’s approach operate orthogonally.

Image Quality Table 3 also demonstrates the rendered images quality metrics across all methods. We observe negligible differences in PSNR, SSIM, and LPIPS metrics between each method’s original implementation and its TC-GS-enhanced counterpart. The minimal variations observed likely originate from hardware-level instruction set disparities and floating-point precision conversion artifacts in the rasterization pipeline.

5.3 Ablation Study

To clearly illustrate the impact of G2L on rendering quality and performance, we ran the following comparisons shown in Table 5 and the rendering images are shown in Fig.6. The ablation experiment shows that all Tensor Core variants boosted FPS. However, direct TF32 computation already introduced noticeable image-quality degradation, and FP16 alone dropped PSNR to just 8 dB. In contrast, combining FP16 Tensor Core optimization with Local Coordinates method preserved nearly same image quality while delivering the highest FPS. This demonstrates that our G2L can simultaneously maximize performance and maintain rendering fidelity.

Table 5: Ablation study on applying TC-GS on original 3DGS.

frag2Mat	G2L	Precision	drjohnson		truck	
			PSNR \uparrow	FPS \uparrow	PSNR \uparrow	FPS \uparrow
		FP32	29.48	108.123	25.44	169.834
✓		FP16	8.85	253.79	6.24	356.619
✓		TF32	20.02	181.429	14.27	290.047
✓	✓	FP16	29.46	253.77	25.44	361.839



Figure 6: Ablation study on G2L when applying TC-GS on original 3DGS.

5.4 Discussion

5.4.1 Limitations

While our method achieves significant acceleration in rendering computations, further optimization could be attained by adopting pipeline techniques similar to those proposed in FlashGS. However, unlike FlashGS’s thread-level pipelining, a warp-level pipelining approach is required. Notably, post-optimization profiling reveals an increased proportion of preprocess overhead in the forward procedure. This preprocess phase inherently involves numerous matrix-based operations such as view transformations, providing opportunities for optimization using Tensor Cores.

5.4.2 Training

Although TC-GS is primarily designed to optimize real-time rendering, our implementation serves as a plug-and-play accelerator for both inference and training, requiring no modifications to the original 3DGS model or the training process.

6 Conclusion

In this paper, we propose TC-GS, a high-performance rendering module for accelerating 3D Gaussian Splatting. TC-GS optimizes the rendering pipeline by decomposing alpha-blending into two components, i.e., Gaussian-related and pixel-related matrices. Through reformulating alpha-blending as matrix multiplications, TC-GS achieves a significant speedup of $2.03\times$ to $4.76\times$ for alpha blending on Tensor Cores. When integrated into state-of-the-art pipelines, TC-GS attains approximately a $2\times$ throughput improvement; even when compared against highly optimized, software-pipelined methods, it delivers a $1.38\times$ speed-up. These gains are realized without any degradation in image quality, demonstrating TC-GS’s superior performance, scalability, and broad applicability for future real-time neural rendering systems.

References

- [1] Saswat Subhajyoti Mallick, Rahul Goel, Bernhard Kerbl, Markus Steinberger, Francisco Vicente Carrasco, and Fernando De La Torre. Taming 3dgs: High-quality radiance fields with limited resources. In *SIGGRAPH Asia 2024 Conference Papers*, pages 1–11, 2024.

- [2] Sankeerth Durvasula, Adrian Zhao, Fan Chen, Ruofan Liang, Pawan Kumar Sanjaya, and Nandita Vijaykumar. Distwar: Fast differentiable rendering on raster-based rendering pipelines. *arXiv preprint arXiv:2401.05345*, 2023.
- [3] Tao Lu, Mulin Yu, Linning Xu, Yuanbo Xiangli, Limin Wang, Dahua Lin, and Bo Dai. Scaffold-gs: Structured 3d gaussians for view-adaptive rendering. In *Proceedings of the IEEE/CVF Conference on Computer Vision and Pattern Recognition*, pages 20654–20664, 2024.
- [4] Kerui Ren, Lihan Jiang, Tao Lu, Mulin Yu, Linning Xu, Zhangkai Ni, and Bo Dai. Octree-gs: Towards consistent real-time rendering with lod-structured 3d gaussians. *arXiv preprint arXiv:2403.17898*, 2024.
- [5] Ying Jiang, Chang Yu, Tianyi Xie, Xuan Li, Yutao Feng, Huamin Wang, Minchen Li, Henry Lau, Feng Gao, Yin Yang, et al. Vr-gs: A physical dynamics-aware interactive gaussian splatting system in virtual reality. In *ACM SIGGRAPH 2024 Conference Papers*, pages 1–1, 2024.
- [6] Xinzhe Wang, Ran Yi, and Lizhuang Ma. Atr-gaussian: Accelerating gaussian splatting with adaptive radius. In *SIGGRAPH Asia 2024 Conference Papers*, pages 1–10, 2024.
- [7] Guofeng Feng, Siyan Chen, Rong Fu, Zimu Liao, Yi Wang, Tao Liu, Zhilin Pei, Hengjie Li, Xingcheng Zhang, and Bo Dai. Flashgs: Efficient 3d gaussian splatting for large-scale and high-resolution rendering. *arXiv preprint arXiv:2408.07967*, 2024.
- [8] Alex Hanson, Allen Tu, Geng Lin, Vasu Singla, Matthias Zwicker, and Tom Goldstein. Speedy-splat: Fast 3d gaussian splatting with sparse pixels and sparse primitives. *arXiv preprint arXiv:2412.00578*, 2024.
- [9] Xiaotong Huang, He Zhu, Zihan Liu, Weikai Lin, Xiaohong Liu, Zhezhi He, Jingwen Leng, Minyi Guo, and Yu Feng. Seele: A unified acceleration framework for real-time gaussian splatting. *arXiv preprint arXiv:2503.05168*, 2025.
- [10] Vickie Ye, Ruilong Li, Justin Kerr, Matias Turkulainen, Brent Yi, Zhuoyang Pan, Otto Seiskari, Jianbo Ye, Jeffrey Hu, Matthew Tancik, et al. gsplat: An open-source library for gaussian splatting. *Journal of Machine Learning Research*, 26(34):1–17, 2025.
- [11] Zhiwen Fan, Wenyan Cong, Kairun Wen, Kevin Wang, Jian Zhang, Xinghao Ding, Danfei Xu, Boris Ivanovic, Marco Pavone, Georgios Pavlakos, et al. Instantsplat: Unbounded sparse-view pose-free gaussian splatting in 40 seconds. *arXiv preprint arXiv:2403.20309*, 2(3):4, 2024.
- [12] Ashish Vaswani, Noam Shazeer, Niki Parmar, Jakob Uszkoreit, Llion Jones, Aidan N Gomez, Łukasz Kaiser, and Illia Polosukhin. Attention is all you need. *Advances in neural information processing systems*, 30, 2017.
- [13] Bernhard Kerbl, Georgios Kopanas, Thomas Leimkühler, and George Drettakis. 3d gaussian splatting for real-time radiance field rendering. *ACM Trans. Graph.*, 42(4):139–1, 2023.
- [14] Xiaoyu Zhou, Zhiwei Lin, Xiaojun Shan, Yongtao Wang, Deqing Sun, and Ming-Hsuan Yang. Drivinggaussian: Composite gaussian splatting for surrounding dynamic autonomous driving scenes. In *Proceedings of the IEEE/CVF conference on computer vision and pattern recognition*, pages 21634–21643, 2024.
- [15] Siting Zhu, Guangming Wang, Xin Kong, Dezhi Kong, and Hesheng Wang. 3d gaussian splatting in robotics: A survey. *arXiv preprint arXiv:2410.12262*, 2024.
- [16] Joo Chan Lee, Daniel Rho, Xiangyu Sun, Jong Hwan Ko, and Eunbyung Park. Compact 3d gaussian representation for radiance field. In *Proceedings of the IEEE/CVF Conference on Computer Vision and Pattern Recognition*, pages 21719–21728, 2024.
- [17] Hao Gui, Lin Hu, Rui Chen, Mingxiao Huang, Yuxin Yin, Jin Yang, Yong Wu, Chen Liu, Zhongxu Sun, Xueyang Zhang, et al. Balanced 3dgs: Gaussian-wise parallelism rendering with fine-grained tiling. *arXiv preprint arXiv:2412.17378*, 2024.
- [18] Jack Choquette, Wishwesh Gandhi, Olivier Giroux, Nick Stam, and Ronny Krashinsky. Nvidia a100 tensor core gpu: Performance and innovation. *IEEE Micro*, 41(2):29–35, 2021.
- [19] Abdul Dakkak, Cheng Li, Jinjun Xiong, Isaac Gelado, and Wen-mei Hwu. Accelerating reduction and scan using tensor core units. In *Proceedings of the ACM International Conference on Supercomputing*, pages 46–57, 2019.
- [20] Abdul Dakkak, Cheng Li, Jinjun Xiong, Isaac Gelado, and Wen-mei Hwu. Accelerating reduction and scan using tensor core units. In *Proceedings of the ACM International Conference on Supercomputing*, ICS ’19, page 46–57, New York, NY, USA, 2019. Association for Computing Machinery.
- [21] Xiaoyan Liu, Yi Liu, Hailong Yang, Jianjin Liao, Mingzhen Li, Zhongzhi Luan, and Depei Qian. Toward accelerated stencil computation by adapting tensor core unit on gpu. In *Proceedings of the 36th ACM International Conference on Supercomputing*, pages 1–12, 2022.

- [22] Jonathan T Barron, Ben Mildenhall, Dor Verbin, Pratul P Srinivasan, and Peter Hedman. Mip-nerf 360: Unbounded anti-aliased neural radiance fields. In *Proceedings of the IEEE/CVF conference on computer vision and pattern recognition*, pages 5470–5479, 2022.
- [23] Arno Knapitsch, Jaesik Park, Qian-Yi Zhou, and Vladlen Koltun. Tanks and temples: Benchmarking large-scale scene reconstruction. *ACM Transactions on Graphics (ToG)*, 36(4):1–13, 2017.
- [24] Peter Hedman, Julien Philip, True Price, Jan-Michael Frahm, George Drettakis, and Gabriel Brostow. Deep blending for free-viewpoint image-based rendering. *ACM Transactions on Graphics (ToG)*, 37(6):1–15, 2018.

A Notations

To clearly present the various parameters and their definitions involved in this paper, the following parameter table lists each symbol along with its corresponding meaning, facilitating readers' understanding of the subsequent analysis and computational processes.

Notation	Meaning	Notation	Meaning
\mathcal{G}	Set of all 3D Gaussian	G	3D Gaussian
P	Number of 3D Gaussians	μ	Mean of 3D Gaussian
Σ	Covariance of Covariance	o	Opacity of 3D Gaussian
c	Color of 3D Gaussian, only in Section 3	W	Matrix projecting 3D position into 2D plane
J	Jacobian of projection	μ'	Mean of projected Gaussian
Σ'	Covariance of projected Gaussian	G'	Projected Gaussian
\mathcal{G}'	Set of projected Gaussians	p	Pixel
\mathcal{T}	Tile, containing pixels	\mathcal{S}	Screen space, containing all tiles
C	Rendered pixel color	α	Opacity of fragments.
T	Transmissivity of fragments.	$n(\mathcal{T})$	Number of splats on tile \mathcal{T}
N	Number of splats.	\mathcal{E}	Complexity of the pipeline in 3DGS
w	Width of the screen	h	Height of the screen
\mathcal{E}_p	Complexity of preprocessing	\mathcal{E}_s	Complexity of sorting
\mathcal{E}_a	Complexity of alpha-blending	k_α	Computation amount in alpha computation
k_{cull}	Computation amount in culling	k_{blend}	Computation amount in blending
f_{cull}	Number of culled fragments	f_{blend}	Number of blended (shaded) fragments.
f_{skip}	Number of skipped fragments	\mathcal{C}	Total computation amount in alpha-blending.
\mathbf{u}	Pixel vector	\mathbf{v}	Gaussian vector
$\begin{bmatrix} a & b \\ b & c \end{bmatrix}$	Σ' , in Section 4 and Appendix B	(μ'_x, μ'_y)	Coordinates of project mean μ'
(p_x, p_y)	Coordinates of pixel p	β	$\ln(\alpha)$, the exponent
\mathbf{U}	Pixel matrix	\mathbf{V}	Gaussian matrix
\mathbf{B}	Exponent matrix	$p(\mathcal{T})$	Center of tile \mathcal{T}
Δp	Pixel in local coordinates	$\Delta \mu'$	Projected mean in local coordinates
r	Arbitrary real number	$H(r)$	r in half-precision presentation.
ϵ_H	Machine epsilon of half precision	ϵ_F	Machine epsilon of single precision
$\hat{\beta}$	Computed β with TC-GS.	S	The upper bound of the rounding error of β
S_1	The rounding error from \mathbf{u}	S_2	The rounding error from \mathbf{v}
λ_1, λ_2	Eigenvalues of Σ'	\mathbf{v}_Δ	Gaussian vector in local coordinates

Table 6: Symbols used in this paper.

B Derivation of the Upper Bound of Rounding Error on TC-GS

We only consider the exponent β in fragment which is not culled, otherwise it will not contribute the pixel color. Besides, we suppose that if a Gaussian will be rendered, each axis of its ellipse is greater than 0.5.

B.1 Rounding Error on Global Coordinates

For an arbitrary real number $r \in \mathbb{R}$ with half-precision point representation $H(r)$, the rounding error can be the estimated by

$$|H(r) - r| \leq |r|\epsilon_H, \quad (20)$$

where $\epsilon_H \approx 9.77 \times 10^{-4}$ is the machine epsilon of FP16 or TF32. We can

In Tensor Cores, the products of two half-precision floating-point numbers $H(r_1), H(r_2)$ is stored as FP32. Therefore, the rounding error of the product satisfies that

$$|H(r_1)H(r_2) - r_1r_2| \leq |r_1r_2|\epsilon_F + |r_1|\epsilon_H + |r_2|\epsilon_H + O(\epsilon_H^2), \quad (21)$$

where ϵ_F is the machine error of FP32. To simply our analysis, we ignore the smaller machine error ϵ_F and quadratic term ϵ_H^2 . Therefore, the rounding error of the product satisfies that

$$|H(r_1)H(r_2) - r_1r_2| \leq (|r_1| + |r_2|)\epsilon_H \quad (22)$$

Then, we delve into the vector product performed by Tensor Cores. Consider an arbitrary vectors $\mathbf{r}, \mathbf{s} \in \mathbb{R}^n$. Since the accumulation is performed on FP32, the rounding error is ignored here. Therefore, the addition only transfer and accumulate the previous rounding error:

$$|H(\mathbf{r}^T)H(\mathbf{s}) - \mathbf{r}^T \mathbf{s}| \leq \epsilon_H \sum_{i=1}^n (|r_i| + |s_i|). \quad (23)$$

The upper bound of rounding error of the exponent $\beta = \mathbf{u}^T \mathbf{v}$ in Section 4 is

$$\begin{aligned} |\hat{\beta} - \beta| &\leq S = S_1 + S_2 \\ S_1 &= \epsilon_H \sup_{p \in [0, w] \times [0, h]} (1 + |p_x| + |p_y| + |p_x^2| + |p_x p_y| + |p_y|^2) \\ S_2 &= \epsilon_H \sup_{G' \in \mathcal{G}'} \sum_{i=0}^5 |v_i(G')|, \end{aligned} \quad (24)$$

where $\mathbf{v}(G')$ is the Gaussian vector of projected Gaussian G' .

Noticing that $S_2 \geq 0$, therefore we have derived a lower bound of the upper bound S :

$$S \geq S_1 \geq \epsilon_H \cdot (h^2 + hw + w^2). \quad (25)$$

We can conclude that

$$S \geq O(h^2 + hw + w^2). \quad (26)$$

The quadratic term of h, w significantly contributes the rounding error. if taking the screen resolution of 720p, i.e., 1280×720 , the upper bound exceeds

$$S \geq S_1 \geq 3 \times 10^3 \quad (27)$$

To compute the relative error, we will find the range of β , which is not culled:

$$\frac{1}{255} \leq \exp(\beta) \leq 1, \quad (28)$$

then $\beta \in [-\ln(255), 0]$, then the relative error exceeds:

$$\Delta \geq \frac{S}{|-\ln(255)|} \geq \frac{S_1}{\ln(255)} > 37500\% \quad (29)$$

B.2 Rounding Error on Local Coordinates

If applying local Coordinates, the term S_1 is

$$S_1 = \epsilon_H \sup_{\Delta p \in [-8, 8]^2} (1 + |\Delta p_x| + |\Delta p_y| + |\Delta p_x^2| + |\Delta p_x \Delta p_y| + |\Delta p_y|^2). \quad (30)$$

Then we can numerically calculate the value of S_1 :

$$S_1 = \epsilon_H (1 + 8 + 8 + 8^2 + 8^2 + 8^2) = 0.204 = O(1). \quad (31)$$

Then we will analyze the other contributor of the upper bound S, S_2 .

At first we find the range of the primitives of projected Gaussians:

Means at local coordinates $\Delta \mu$: Since the coordinate will be left or upside of the tile center, the coordinate value can be negative. Therefore, $\Delta p \in [-w, w] \times [-h, h]$.

logarithm of opacity $-\log(o)$: In implementation, the opacity $o < \frac{1}{255}$ will be pruned at the preprocessing stage, therefore $-\log(o) \in [-\ln(255), 0]$.

Inverse covariance $\Sigma'^{-1} = \begin{bmatrix} a & b \\ b & c \end{bmatrix}$ At first we assume that the major and the minor axis of the ellipse are larger than 0.5, otherwise it will not be rendered. Then the eigenvalues of the projected covariance Σ' is greater than 0.5:

$$\lambda_1, \lambda_2 \geq 0.5. \quad (32)$$

And the eigenvalues of the inverse covariance Σ'^{-1} satisfies:

$$0 < \lambda_1^{-1}, \lambda_2^{-1} \leq 2. \quad (33)$$

Consider the characteristic polynomial of Σ'^{-1} :

$$f(\lambda) = |\lambda I - \Sigma'^{-1}| = \lambda^2 - (a + c)\lambda + ac - b^2. \quad (34)$$

These two eigenvalue are the roots of $f(\lambda) = 0$, and:

$$\lambda_1^{-1} + \lambda_2^{-1} \in (0, 4], \quad \lambda_1^{-1} \lambda_2^{-1} \in (0, 4]. \quad (35)$$

Applying Vieta's formulas:

$$a + c \in (0, 4], \quad ac - b^2 \in (0, 4]. \quad (36)$$

Since $ac - b^2 \geq 0$, then $ac \geq b^2 \geq 0$. Therefore, we can conclude that:

$$0 < a \leq 4, \quad 0 < c \leq 4, \quad (37)$$

and

$$b^2 \leq 4 + ac \leq 4 + \left(\frac{a+c}{2}\right)^2 \leq 8, \quad (38)$$

$$-2\sqrt{2} \leq b \leq 2\sqrt{2}. \quad (39)$$

To simply the notation, we note $\mathbf{v}_\Delta = [v_0, v_1, v_2, v_3, v_4, v_5]^T$ Next, we can compute the term S_2 :

$$\begin{aligned} S_2 &= \epsilon_H \sup(|v_0| + |v_1| + |v_2| + |v_3| + |v_4| + |v_5|) \\ &= \epsilon_H \sup(|v_0|) + \epsilon_H(2\sqrt{2} + 4)(h + w + 1) \\ &= \epsilon_H \sup(|v_0|) + O(h + w). \end{aligned} \quad (40)$$

Therefore, we can conclude that:

$$S = S_1 + S_2 = \epsilon_H \sup(|v_0|) + O(h + w). \quad (41)$$

Then we turn to bound the value of β :

$$\begin{aligned} \beta &= v_0 + \Delta p_x v_1 + \Delta p_y v_2 + \Delta p_x^2 v_3 + \Delta p_x \Delta p_y v_4 + \Delta p_y^2 v_5 \\ &= v_0 + O(h + w) + O(h + w) + O(1) + O(1) + O(1) \\ &= v_0 + O(h + w) \end{aligned} \quad (42)$$

Since we only consider the β value which contributes the pixel color, $\beta \in [-\ln(255), 0]$. Then

$$v_0 = \beta - O(h + w) = O(h + w). \quad (43)$$

Therefore, the upper bound of the of the error of β satisfies

$$|\hat{\beta} - \beta| \leq S = O(h + w) + \epsilon_H O(h + w) = O(h + w). \quad (44)$$

if $\beta \in [-\ln(255), 0]$.